Dislocation mechanism of deuterium retention in tungsten under plasma implantation

2014 J. Phys.: Condens. Matter 26 395001

(http://iopscience.iop.org/0953-8984/26/39/395001)

IOP Publishing Journal of Physics: Condensed Matter
J. Phys.: Condens. Matter **26** (2014) 395001 (10pp) doi:10.1088/0953-8984/26/39/395001

Dislocation mechanism of deuterium retention in tungsten under plasma implantation

V I Dubinko[1], P Grigorev[2,3], A Bakaev[2,5], D Terentyev[2], G van Oost[4], F Gao[5], D Van Neck[6] and E E Zhurkin[7]

[1] National Science Center 'Kharkov Institute of Physics and Technology', Kharkov 61108, Ukraine
[2] SCK•CEN, Boeretang 200, 2400 Mol, Belgium
[3] Ghent University, Applied Physics EA17 FUSION-DC, St. Pietersnieuwstraat 41 B4, B-9000 Ghent, Belgium
[4] Department of Applied Physics, Ghent University, 9000 Ghent, Belgium
[5] Pacific Northwest National Laboratory, Richland, WA 99352, USA
[6] Center for Molecular Modeling, Department of Physics and Astronomy, Ghent University, Technologiepark 903, 9052 Zwijnaarde, Belgium
[7] Department of Experimental Nuclear Physics, Institute of Physics, Nanotechnologies and Telecommunications, St. Petersburg State Polytechnical University, 29 Polytekhnicheskaya street, 195251, St. Petersburg, Russia

E-mail: dterenty@sckcen.be

Received 31 March 2014, revised 28 June 2014
Accepted for publication 4 July 2014
Published 20 August 2014

Abstract

We have developed a new theoretical model for deuterium (D) retention in tungsten-based alloys on the basis of its being trapped at dislocations and transported to the surface via the dislocation network with parameters determined by *ab initio* calculations. The model is used to explain experimentally observed trends of D retention under sub-threshold implantation, which does not produce stable lattice defects to act as traps for D in conventional models. Saturation of D retention with implantation dose and effects due to alloying of tungsten with, e.g. tantalum, are evaluated, and comparison of the model predictions with experimental observations under high-flux plasma implantation conditions is presented.

Keywords: tungsten, retention, plasma

(Some figures may appear in colour only in the online journal)

1. Introduction

The current choice of materials to be used in ITER plasma-facing components includes tungsten (W) and beryllium [1]. The sputtering yield of tungsten is much lower than that of beryllium, while its melting point is significantly higher. However, the practical use of W is hindered by its high ductile-to-brittle transition temperature, and therefore risk of brittleness between plasma pulses in the course of operation. In order to improve the mechanical properties, tungsten alloys are considered. One of the issues still to be clarified is the retention of hydrogen (H) isotopes (including deuterium and radioactive tritium) in tungsten alloys, as the plasma-facing components are supposed to sustain high-flux plasma.

As hydrogen isotope ions are neutralized and thermalized following the implantation, further evolution depends on hydrogen solubility in W – i.e. the energy of H solution in W, which is positive. According to the phase diagram of a W-H system, in the temperature region of 300-1,000 K, relevant for ITER conditions, an equilibrium concentration of H dissolved in α-W ranges from 10^{-18} to 10^{-6} at.% [2]. Above this solubility limit (e.g. under plasma exposure that implants H ions into material), H does not form hydrides with W, but precipitates in the bubbles filled with H_2 molecules [2]. However, the thermodynamic diagram does not indicate the ways of the

bubble formation, which occurs via diffusion, trapping, nucleation and growth. The critical issue here is to determine the mechanisms of trapping and nucleation of H bubbles, which basically define the retention of hydrogen in material.

Recently a significant amount of works have been dedicated to both computational assessment of hydrogen permeation in W (see e.g. [3–6]) and experimental characterization of this phenomenon (see e.g. [7–12]). Experimental investigations of trapping and release of D in pure tungsten (W) and tungsten-tantalum (W-Ta) alloys [6–8] show that there is a considerable amount of trapped D in the bulk within a depth of several microns, which is similar to the case of He trapping in W. However, the essential difference between hydrogen and helium agglomeration in tungsten is that the binding energy between two hydrogen atoms is an order of magnitude lower than that for helium. It means that, in a marked contrast to He, a homogeneous nucleation of D clusters is highly improbable. Accordingly, nucleation of hydrogen clusters requires binding cites. In current models dealing with deuterium (D) retention in tungsten [2], it is argued that the nucleation of D-complexes is determined crucially by the concentration of radiation-produced vacancies, which act as traps for fast-migrating D atoms. One vacancy has been argued to trap up to 5–6 hydrogen atoms [3–5]. At sufficiently low temperatures considered in ref. [2], vacancies are immobile while self-interstitial atoms (SIAs) diffuse and become trapped with impurity atoms (mainly carbon, C) or are absorbed by dislocations. Thus, the result strongly depends on the dislocation density and C-SIA trapping energy, which have to be high enough to trap SIAs so that the remaining vacancies can trap D atoms and act as nucleation cites for D-clusters. This model was developed to describe ion implantation with energies of 5–30 keV, but cannot be applied (even qualitatively) to nucleation of D-clusters at *sub-threshold* implantation conditions, i.e. when the ion energy is too low to produce stable vacancy-SIA pairs in the crystal bulk, and the operating temperature range is too low (<500 K) to induce any significant concentration of thermal vacancies. The sub-threshold implantation conditions are important, however, since they correspond to the plasma-wall interaction regime expected to occur in the ITER and experiments involving high-flux, high-temperature deuterium plasmas with ion energies of up to several tens of eV [6, 7]. Hence, the description of the trapping of D at these irradiation conditions requires alternative mechanisms to those considered in the current models.

In this work, we analyze the trapping of hydrogen on typical microstructural features such as dislocations and compare the efficiency of this mechanism with the homogenous self-trapping mechanism (conventionally considered for helium retention). Based on the available *ab initio* results, we construct a theoretical model to evaluate the retention of D on dislocation lines. The model is then applied to describe thermal desorption spectroscopy (TDS) results, which are used to verify activation energies of deuterium detrapping.

2. Homogeneous self-trapping of deuterium in the bulk

Ab initio calculations [5] show that two hydrogen atoms trap each other weakly with a binding energy E_b ~0.01 eV, (as compared, e.g. with helium forming strong pairs with a binding energy of E_b ~1 eV). Figure 1 shows detrapping frequency, w_{de}, for D-D pairs based on these estimates, as compared to trapping frequency, w_{DD}, i.e. the frequency of collisions of one D atom with others having concentrations of C_D^b in the crystal bulk, given by the following expressions:

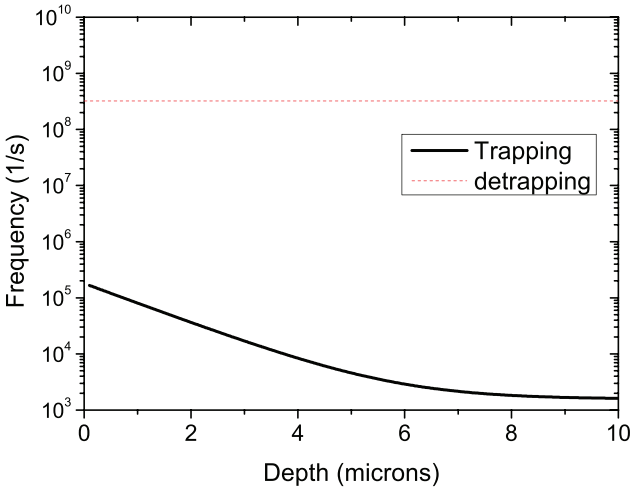

Figure 1. Trapping and detrapping frequency for D-D pairs in W bulk as a function of depth. Implantation conditions correspond to those applied in [6, 7], i.e. D flux $F_D = 10^{20}\,\mathrm{m^{-2}s^{-1}}$ and temperature T = 460 K.

$$w_{DD} = \alpha_{DD} C_D^b, \quad \alpha_{DD} = \frac{4\pi}{\omega}\left(\frac{3\omega}{4\pi}\right)^{1/3} D_D^b, \tag{1}$$

$$D_D^b \approx b^2 w_0 \exp\left(-\frac{E_m^b}{k_B T}\right), \tag{2}$$

$$w_{\mathrm{de}} = w_0 \exp\left(-\frac{E_b + E_m^b}{k_B T}\right), \quad w_0 = 10^{13} s^{-1}, \tag{3}$$

where $\omega \approx 0.5 b^3$ is the atomic volume, b is the lattice spacing, D_D^b is the bulk diffusion of D atoms, w_0 is the attempt-frequency prefactor, E_m^b is the bulk migration energy and $k_B T$ has the usual meaning.

One can see that the trapping frequency decreases with distance (depth) from the surface due to decreasing C_D^b (see the next section), and it is several orders of magnitude lower than that of detrapping. So a homogeneous nucleation of D (or H) clusters is indeed questionable in such implantation conditions, and one needs an alternative trapping mechanism for D atoms at some intrinsic defects to provide the nucleation sites for the D clustering. Grain boundaries were suggested as nucleation sites for bubbles [9]; however, the retention also takes place in the recrystallized W [10], and even in single crystal W [11]. What is more, the presence of different impurities does not result in any significant difference in the D depth profiles, either [6, 7].

In the next section we consider a model of D retention mediated by dislocations, which are proven to act not only as trapping sites, but also as pathways for preferential D diffusion through bulk. This complex trapping-detrapping D diffusion along dislocation lines results in the removal of D to the exposure surface and in-bulk penetration.

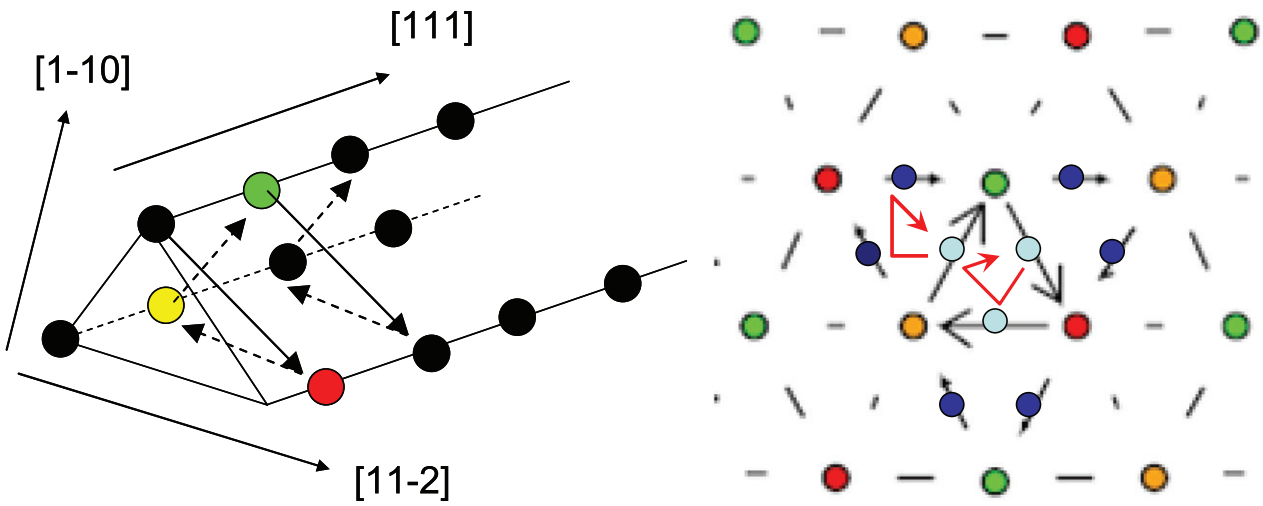

Figure 2. The schematics of core atoms in a ½ < 111 > screw dislocation in 3 D (left figure) and projection onto the (111) plane (right figure). The black arrows indicate the difference between displacements of neighboring < 111 > columns forming the dislocation core. The length of the arrow is proportional to the magnitude of displacement difference, and the direction of the arrow indicates the sign of the displacement difference (i.e. the column that the arrow points to has a larger displacement than the column on the other end of the arrow). Among the three atoms that surround the centre of the dislocation, the arrows form a closed circuit. Note that while the arrows reveal a displacement component in the (1 1 1) plane for convenience of visualization, the displacement component they represent is strictly out of the plane. The three ground state positions in, and six ground state positions next to, the dislocation core are schematically shown in the right figure by light- and dark-blue balls, respectively. The red arrow connecting three light-blue balls reveals the migration path for H inside the SD core. The red arrow connecting one light-blue with two dark-blue balls represents the migration path along the dislocation core.

3. Trapping of hydrogen isotopes mediated by dislocations

3.1. Ab initio calculations

The microstructure of tungsten below 0.1 T_m (melting temperature) is characterized by long $a_0/2 < 111 >$ screw dislocation lines [13], as is usual for BCC metals, where a_0 is the lattice constant. Density functional theory (DFT) calculations have been applied to compute the interaction of D with the screw dislocation (SD) core in our previous work [14]. Here we extend these calculations further to assess H_N-SD interaction for different configurations of hydrogen clusters. We used the Vienna *Ab-Initio* Simulation Package (VASP [15]). The projected augmentation wave [16] and the generalized gradient approximation (GGA [17]) were used for the pseudopotential and the exchange-correlation potential, respectively. The 1s state for H and 5d6s states for W are treated as valence states in the calculations. The atomic relaxation is carried out using the conjugate-gradient algorithm with the force convergence criterion of 0.03 eVÅ^{-1}.

It has been shown that there are at least three positions for D inside the core, in which D is trapped with the binding energy $E_b^1 = 0.6$ eV. In addition, there are six positions for D adjacent to the dislocation core, in which the binding energy is only slightly lower (i.e. being 0.55 eV). The schematic picture showing the core structure of a_0½ < 1 1 1 > screw dislocation and location of D atoms is presented in figure 2. The calculations of the migration barrier between in-core positions provide the migration barrier for the H diffusion along the dislocation line. The two migration paths (inside and adjacent to the SD core, as shown in figure 2) were analyzed, and the resulting migration barrier, E_m^d, was computed to be ~0.1 eV.

The in-core migration energy is essentially lower than the bulk migration energy, $E_m^b = 0.4$ eV [2], which means the travel path of H diffusing along the dislocation line before detrapping, L_d^0, is expected to be significant. The latter can be estimated as follows [18]:

$$L_d^0 = b \exp\left(\frac{E_m^b - E_m^d + E_b^1}{2k_B T}\right), \tag{4}$$

At T < 460 K, L_d^0 exceeds 10 μm (typical size of subgrains in polycrystalline W), implying that D atoms trapped at dislocations will remain until they reach another microstructural feature (e.g. a free surface, dislocation junction or grain boundary). Condensation of migrating D atoms on dislocation lines will result in the formation of D_2 clusters also attached to dislocations, as DFT calculations suggest the presence of the attractive interaction not only for an isolated D, but for small clusters as well [14]. The growth of a D_N cluster starting from D_2 will occur by its extension along the dislocation line. A comparison of the interaction energy of D to a D_{N-1} cluster in different configurations is presented in figure 3. The interaction energies were computed following the standard definition – i.e. as the difference of the total energy corresponding to the states of an atomic system that contains two relevant defects together and apart. Following this definition a negative value of the interaction energy corresponds to the attractive interaction. The expressions for the interaction energy of a D atom with a D_{N-1} cluster located in bulk, or placed on a dislocation or dislocation jog are the following:

$$E(D^D + D_{N-1}^D) = E_N^D + E^D - E_{N-1}^D - E_I^D, \tag{5}$$

$$E(D^B + D_{N-1}^D) = E_N^D + E^B - E_{N-1}^D - E_I^B, \tag{6}$$

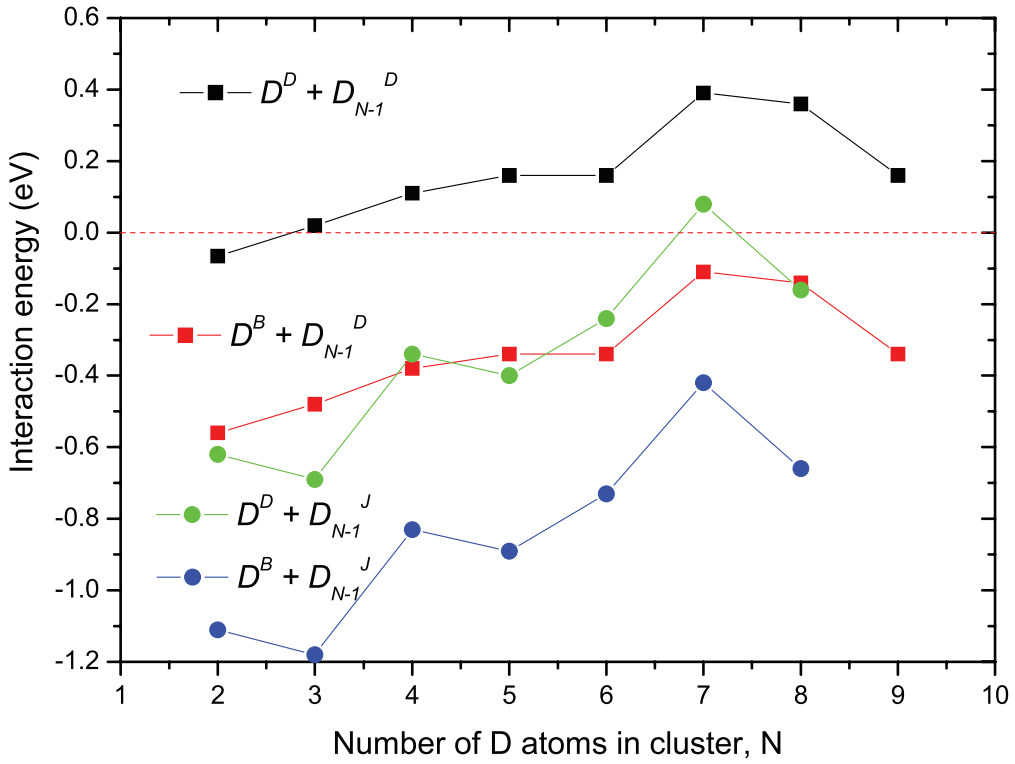

Figure 3. The interaction energy of $D^X - D^Y_{N-1}$, where symbols X and Y imply the location of interstitial D and D_{N-1} clusters. This correspondingly could be B=bulk, D=dislocation, J=jog on dislocation. The interaction energy is measured as the difference of the total energy of configurations, including two objects together and apart. With this notation, the negative value of the interaction energy implies attractive interaction (i.e. positive binding energy). Positive values (for $D^B+D_{N-1}{}^D$) favour dissolution of D_N (for $N > 2$) into smaller ones without leaving the dislocation core, while the formation of D_N on a dislocation jog is an energetically favourable process.

$$E(D^D + D^J_{N-1}) = E^J_N + E^D - E^J_{N-1} - E^D_1, \quad (7)$$

$$E(D^B + D^J_{N-1}) = E^J_N + E^B - E^J_{N-1} - E^B_1, \quad (8)$$

where E^D is the total energy of the crystal containing the screw dislocation (containing m W atoms), and E^B is the total energy of the perfect crystal with the same dimensions and number of W atoms as were used to create the screw dislocation. Cohesive energy of a single W atom, defined as $E_{coh} = E^B/m$; E^B_1, is the total energy of the crystal containing a single interstitial (tetrahedral) hydrogen atom relaxed in a perfect crystal; E^D_1 and E^D_N are the total energy of a crystal containing a single interstitial hydrogen atom or a cluster of N hydrogen atoms placed at the most favourable position(s) on the screw dislocation line and relaxed; E^J_N is the total energy of the crystal containing a cluster of N hydrogen atoms placed in the jog on the screw dislocation.

Results in figure 3 show that on a perfect dislocation line, the accumulation of D clusters into a compact 3 D structure is not a favourable process, and D atoms would prefer to form chains decorating the dislocation core. (Note that D chains also remain trapped by the dislocation). It means that the formation and growth of compact larger D_N clusters will require the presence of nucleation sites, such as jogs or dislocation intersections, in which D atoms will also become immobilized. To validate this hypothesis, we generated a vacancy jog on a screw dislocation line and assessed the interaction of H_N clusters with that jog. The interaction energy of D with a D_{N-1} cluster located on the jog is also given in figure 3 and table 1.

Table 1. The interaction energy of $D^X - D^Y_{N-1}$, where symbols X and Y imply the location of interstitial D and D_{N-1} cluster.

Number of D atoms in cluster	$D^B - D^B_{N-1}$	$D^B - D^D_{N-1}$	$D^B - D^J_{N-1}$	$D^D - D^J_{N-1}$
2	–0.0652	–0.56	–1.11	–0.62
3	0.02	–0.48	–1.18	–0.69
4	0.11	–0.38	–0.83	–0.34
5	0.16	–0.34	–0.89	–0.4
6	0.16	–0.34	–0.73	–0.24
7	0.39	–0.11	–0.42	0.08
8	0.36	–0.14	–0.66	–0.16
9	0.16	–0.34	—	—

The figure shows that a compact cluster can grow (being fed by D coming from both bulk and dislocation core) and accommodate at least eight D atoms.

The D_N clusters formed on jogs can grow and eventually reach a supercritical size, at which they transform into a bubble by emission of secondary jogs that release necessary volume for the cluster, as more D atoms will approach the nucleus. The energetic analysis of this process was performed in [14], where it is suggested that a 'jog-punching' mechanism operates once the cluster size exceeds D_8. (See the relaxed configuration of a D_8 cluster placed on a dislocation jog in figure 4). Once the supercritical size is reached, the cluster will grow as a macroscopic bubble by the classical loop punching mechanism [19]. The dissolution of D bubbles attached to the screw dislocation line may, however, occur by

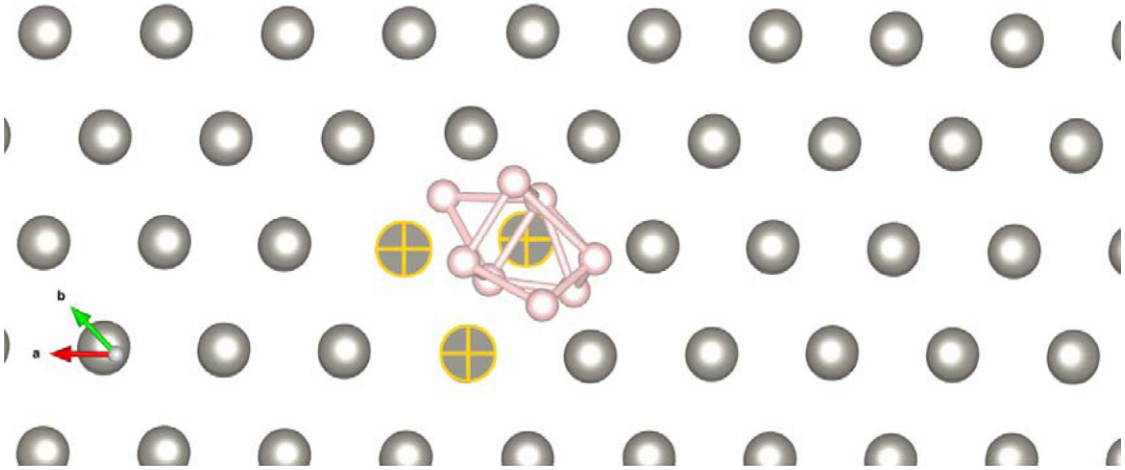

Figure 4. Relaxed configuration of an H_8 cluster formed on the jog in a core of a ½ < 111 > screw dislocation. The dislocation line is oriented normal to the paper, and the three W atoms marked by crosses form the SD core. See the atomic core structure in figure 2.

two channels: (i) emission of D into bulk or (ii) emission of D on a dislocation line. The former is the classical process, and its activation energy can be roughly estimated as the permeation energy (which varies in the range 1.25–2.0 eV following DFT calculations for H in W [5]). Experimentally, the activation energy for this process is deduced to be ~1.5–1.7 eV. (See the section 4). Emission from bubble to dislocation requires a lower energy barrier, since the emitted D would be bound to the dislocation core and the corresponding activation energy is lower by $E_b^1 = 0.6$ eV. Taking the permeation energy from the experimental assessment (~1.6 eV), we shall consider that the activation energy for the D emission from a bubble to the dislocation line is ~ 1 eV. Even though there will be a significant difference in the activation energy for the two emission channels, they will compete with each other as temperature rises (especially at high heating rates typical of TDS measurements, which will be discussed further in section 4). The reason for the competition originates from the essential discrepancy of the effective emission surface, which is higher by a factor of $4\pi R^2/2a_0^2$ for the bulk emission as compared to the emission directly on the dislocation line. Hence, the first emission channel will also operate especially for large bubbles and at high temperature.

Based on the above-presented DFT results, a model for D trapping, transport by dislocation network (accounting for D clustering along the dislocation lines) and detrapping at typical TDS conditions is described in the following.

3.2. Rate theory of D trapping and transport

The model of D-cluster nucleation and growth at dislocation junctions is sketched in figure 5. The upper figure shows W samples exposed to high-flux D plasma [7, 8] being inspected by transmission electron microscopy (TEM [13]). A typical dark field image shows screw dislocation lines decorated by cavities (presumably D bubbles, as such features were not detected in the pre-exposed samples). The amount of visible hydrogen clusters is rather low for an accurate statistical determination, but based on the inspection of a considerable number of images, a mean linear spacing of 100 ± 20 nm was obtained. The lower picture illustrates a mechanism of D-transport via the dislocation network, in which junctions act as nucleation sites for D-clusters. The exposure surface is on the left-hand side.

The trapping rate of an N_{th} atom by a D_{N-1} cluster $w_n^+(x)$ formed at such a nucleation site at the depth x can be estimated as the product of the D flux from the bulk to the unit length of the dislocation J_d^D, and the length along the dislocation, from which each cluster is fed with migrating D-atoms, L_d:

$$w_n^+(x,\,t) = J_d^D L_d, \quad J_d^D = \frac{Z_d}{\omega} D_D^b \left[C_D^b(x,\,t) - C_d^{th}\right], \qquad C_d^{th} = \exp\left(-\frac{E_b^1}{k_B T}\right), \tag{9}$$

where $Z_d \sim 1$ is the dislocation capture efficiency for D-atoms from the bulk [20], $C_D^b(x)$ is the mean bulk D-concentration determined by trapping at dislocations, and C_d^{th} is the thermal equilibrium concentration determined by detrapping from dislocations. The maximum value of L_d is determined by equation 4 (figure 3), but in reality it should be limited by the mean distance between the clusters.

The bulk D-concentration $C_D^b(x,\,t)$ depends on the distance from the implanted surface, and can be evaluated by solving diffusion problems in the effective medium (see e.g. [20]), in which dislocations are the dominant sinks for D atoms implanted at the surface ($x = 0$):

$$\frac{\partial C_D^b}{\partial t} = D_D^b \frac{\mathrm{d}^2 C_D^b(x,\,t)}{\mathrm{d}x^2} - k_D^2 D_D^b \left[C_D^b(x,\,t) - C_d^{th}\right], \qquad k_D \approx \left(Z_d \rho_d\right)^{0.5}, \tag{10}$$

$$C_D^b(0,\,t) = \frac{\omega F_D X_D}{D_D^b} \equiv C_D^b(0), \; C_D^b(\infty,\,t) = C_d^{th}, \tag{11}$$

where ρ_d is the dislocation density. D concentration at the surface $C_D^b(0,\,t)$ is determined by the implantation flux F_D, straggling X_D, and D-atom mobility, while deep in the bulk it is assumed to be in thermal equilibrium with respect to detrapping from dislocations.

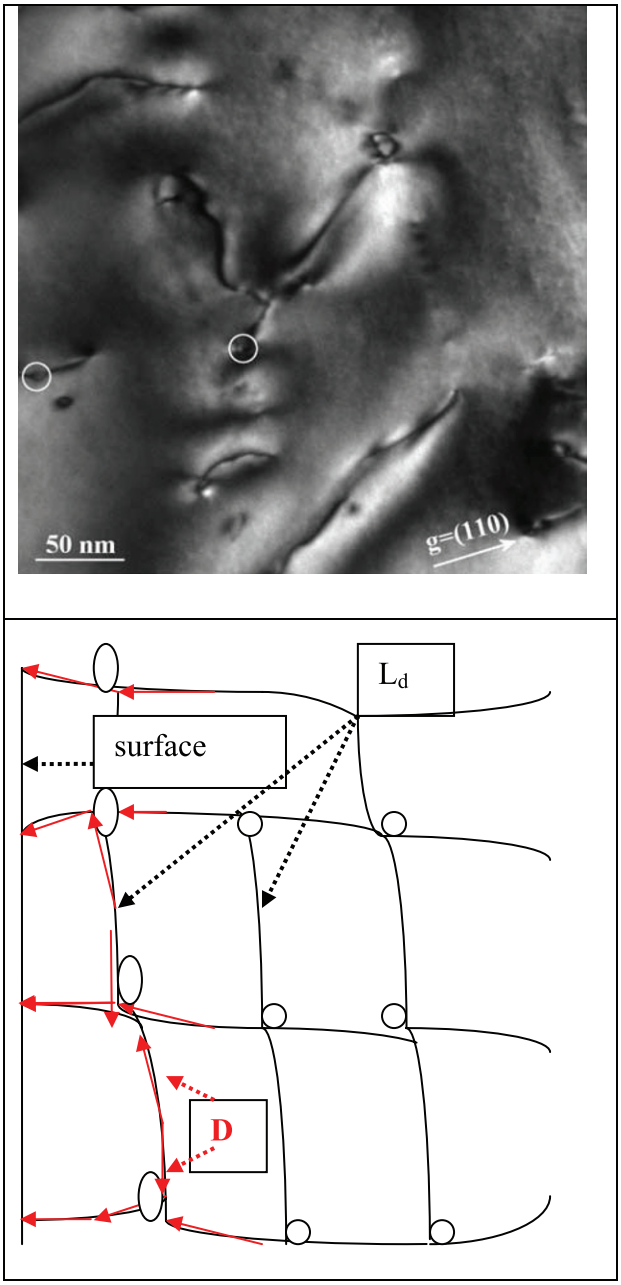

Figure 5. Dark field TEM image of screw dislocations decorated by D clusters (two examples are indicated by the white circles [14]), and schematic illustration of D-transport via the dislocation network with D-clusters separated by dislocation segments L_d.

At times larger than diffusion times through the region of interest (~1 s for 10 micron depth at an implantation temperature of 460 K), a steady-state profile of $C_D^b(x)$ is established, which is given by:

$$C_D^b(x) - C_d^{th} = \left[C_D^b(0) - C_d^{th}\right]\exp(-xk_D). \qquad (12)$$

The concentration profile is shown in figure 6(*a*) for different dislocation densities ranging from annealed to cold worked state. It is significantly lower than the profile of the D retention measured experimentally [7–9] (figure 6(*b*)), which implies that the transport of D atoms along dislocations to the surface should be lower than the transport in the bulk. This could be accomplished via formation of traps – stable D-clusters attached to dislocations, in the vicinity of which the activation energy for D migration is significantly enhanced compared to that in a 'bare' dislocation core.

Let us evaluate a steady-state profile of the concentration of D atoms attached to dislocation, which is determined by the balance between D absorption from the bulk and migration along the core:

$$\frac{\partial C_D^d(x)}{\partial t} = \left(\frac{\mathrm{d}C_D^d(x)}{\mathrm{d}t}\right)_b - D_D^d\frac{\mathrm{d}^2C_D^d(x)}{\mathrm{d}x^2} = 0, \qquad (13)$$

$$C_D^d(0) = C_D^b(0)\frac{D_D^b}{D_D^d},\ C_D^b(\infty) = C_d^{th}, \qquad (14)$$

$$\left(\frac{dC_D^d(x)}{dt}\right)_b = Z_d\rho_d D_D^b\left[C_D^b(x) - C_d^{th}\right]. \qquad (15)$$

The solution of equation (13) with boundary conditions (14) is given simply by:

$$C_D^d(x) - C_d^{th} = \frac{D_D^b}{D_D^d}\left[C_D^b(0) - C_d^{th}\right]\exp(-xk_D) \qquad (16)$$

which differs from the bulk concentration (12) only by the ratio of the bulk-to-dislocation diffusion coefficients D_D^b/D_D^d. Let us estimate D_D^d by the following expression:

$$D_D^d = \frac{L_d^2}{\tau_d}$$

which assumes that migration along the dislocation occurs by quick 'jumps' (i.e. fast diffusion) between the D-clusters attached to the core at spacing L_d, from which D atoms can escape with an effective activation energy E_m^{eff}. Figure 6 shows the resulting profiles for the bulk concentration and retention of D at dislocations, taking E_m^{eff}=1 eV and different cluster spacing ranging from 250 to 80 nm. Decreasing L_d may be attributed to the increasing concentration of D-clusters with implantation time rising from 70 to 1,400 s. The choice of $E_m^{\mathrm{eff}}$is motivated by the discussion provided in the previous section and the estimation of the activation energy for the D emission from a bubble attached to a dislocation line. (See also the discussion in section 3).

Now let us estimate the mean cluster radius corresponding to the D retention at dislocations, which is given by the deuterium balance equation and shown in figure 7:

$$R_C(x) = \left(\frac{3L_dC_D^d(x)}{4\pi\rho_d n_{Dv}}\right)^{1/3}, \qquad (18)$$

where $n_{Dv} \approx 5$ is the number of D atoms per vacancy in the cluster, which is estimated from DFT calculations showing that a vacancy can trap up to 5–6 hydrogen atoms [4–6].

Now the total D retention can be evaluated by integrating $C_D^d(x)$ over the depth, x, up to the depth L, from which deuterium can reach the surface during TDS: $\mathrm{Re}_D^d = \int_0^L C_D^d(x)\mathrm{d}x$.

If one assumes the following decrease of spacing L_d with implantation time due to nucleation of new clusters, which saturates at 80 nm (figure 8) in accordance with TEM observations (figure 5), then the retention first increases and subsequently saturates, as shown in figure 9.

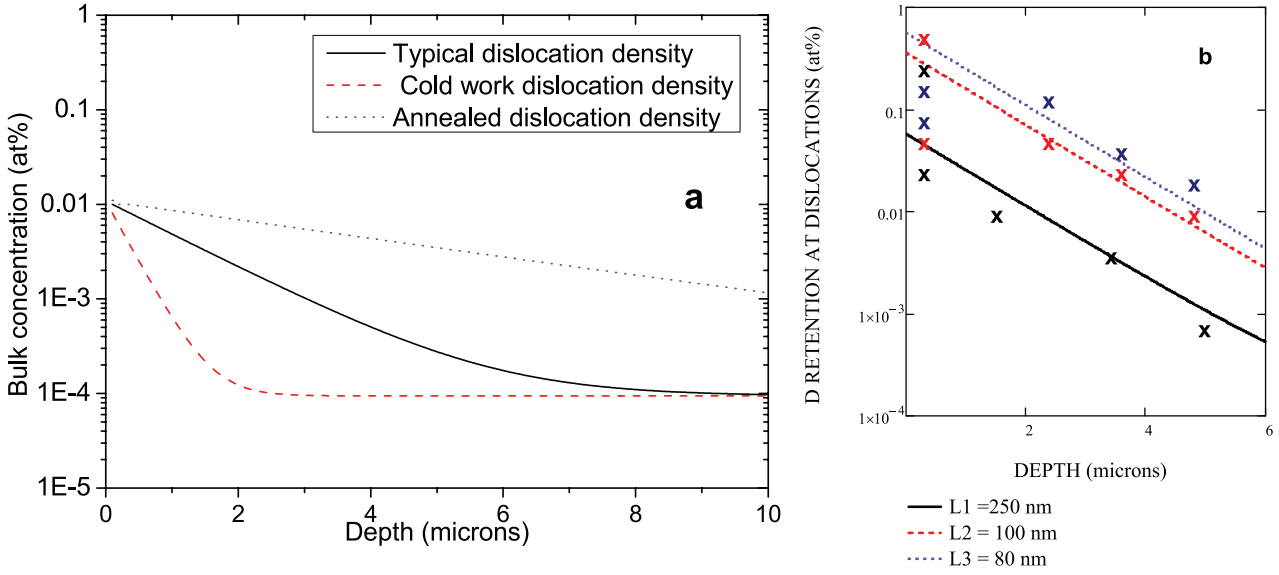

Figure 6. (*a*) Steady-state profile of the concentration of D atoms in the bulk, determined by trapping at dislocations with the following densities: annealed $\rho_d = 0.5 \times 10^{11}\,\mathrm{m}^{-2}$, typical $\rho_d = 0.5 \times 10^{12}\,\mathrm{m}^{-2}$, cold worked $\rho_d = 0.5 \times 10^{13}\,\mathrm{m}^{-2}$. (*b*) D retention at dislocations at $\rho_d = 0.5 \times 10^{12}\,\mathrm{m}^{-2}$. Implantation conditions [7, 8]: $F_D = 10^{20}\,\mathrm{m}^{-2}\mathrm{s}^{-1}$, X_D = b, T = 460 K. Experimental data is shown for different implantation times ranging from 70 s (black); 490 s (red) 1,400 s (blue).

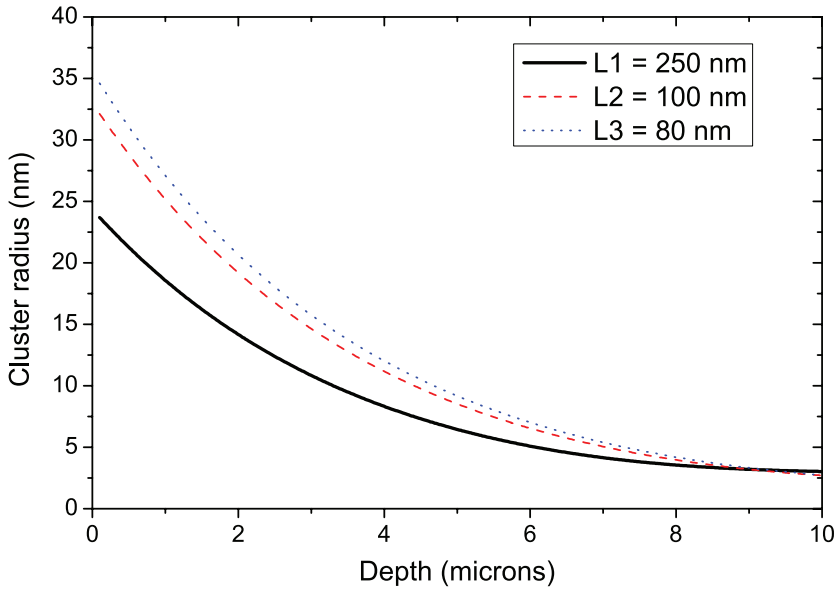

Figure 7. Mean cluster radius corresponding to the D retention at dislocations presented in figure 6(*b*).

The comparison with experimental data shows that the present model can account for the observed saturation of the D retention with implantation time that adjusts itself adiabatically to changing cluster structure. Alloying W with Ta has been shown to increase dislocation density [12], which can explain the observed decrease in the total retention in the W-Ta alloys compared to pure W.

4. Analysis of TDS results

In order to verify activation energies used in the present model, let us consider results of thermal desorption spectroscopy (TDS [7]) shown in figure 10(*a*). The rate of deuterium release was measured as the sample temperature was increased at a constant rate 0.5 K/s, which the defined characteristic time of the temperature change as $\tau_T \approx 2$s. During this time, deuterium can be transported to the surface via dislocation network from a depth $x = \sqrt{D_D^d \tau_T}$, which allows one to estimate the dependence of the desorption temperature on the depth and desorption activation energy E_m^{eff} as follows:

$$T_{de}(x) = \frac{E_m^{\mathrm{eff}}}{\ln(w_0 \tau_T L_d^2 / x^2)}. \qquad (20)$$

Figure 10(*b*) shows that desorption temperature ranges from 450 to 700 K, with depth increasing from 1 nm to 1 micron, taking E_m^{eff} =1 eV. The profile of retained deuterium

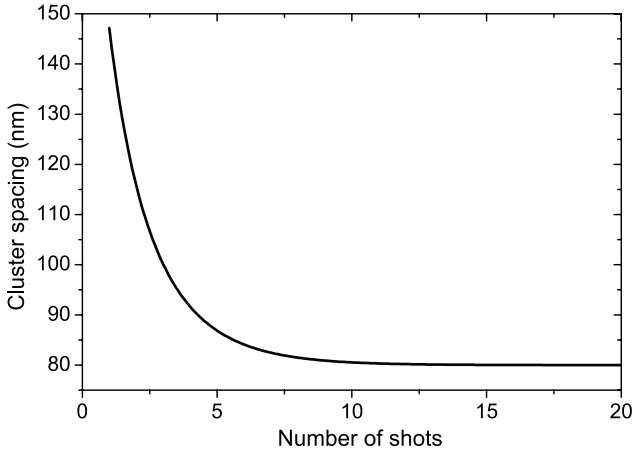

Figure 8. Cluster spacing fitted to describe saturation of the total D retention with implantation 'shots' (1 shot = 70 s) given by fit $L_d(N) = 80nm{\cdot}\exp\{\exp[-0.5(N-0.1)]\}$.

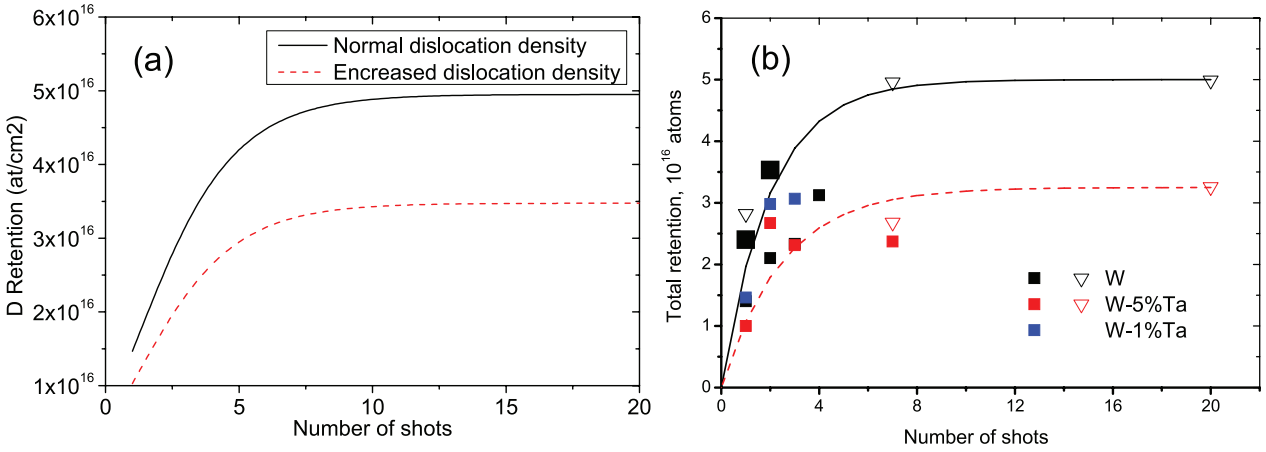

Figure 9. Total D retention versus the number of shots at different dislocation densities: (*a*) normal $\rho_d = 0.5 \times 10^{12}\,\mathrm{m}^{-2}$, increased $\rho_d = 10^{12}\,\mathrm{m}^{-2}$ versus (*b*) experimental data [8] for W, W-1%Ta and W-5%Ta. Hollow symbols correspond to accumulating exposures, filled symbols – to the exposures where TDS measurements were performed after each shot. The lines are to guide the eye.

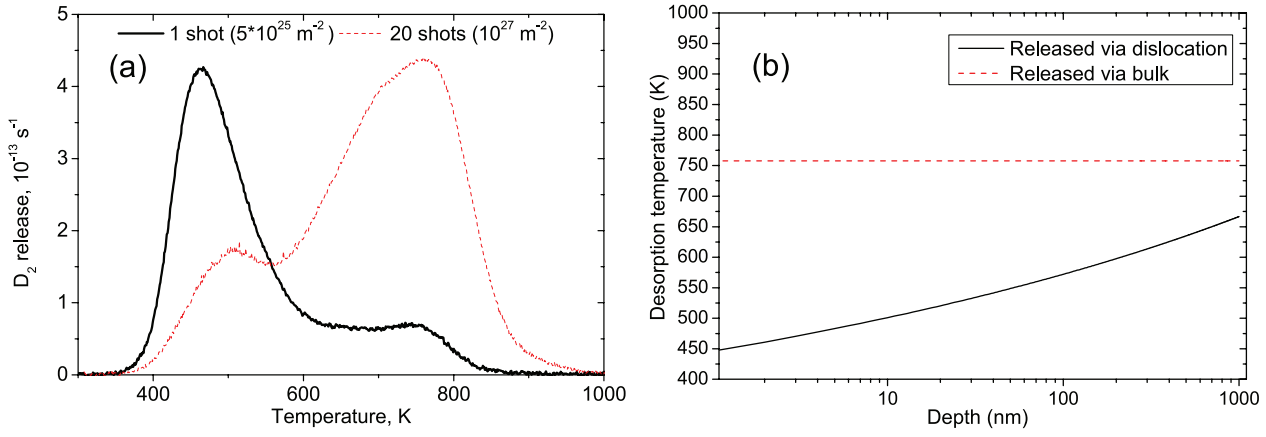

Figure 10. (*a*) TDS spectra of the W sample after exposures to 1 plasma shot (70 s) and 20 shots at high deuterium flux $F_D = 10^{20}\,\mathrm{m}^{-2}\mathrm{s}^{-1}$ [7]. (*b*) Calculated dependence of the temperature of desorption via dislocations on the depth, assuming $E_m^{\mathrm{eff}} = 1$ eV, versus the temperature of desorption via bulk, assuming the activation energy of 2 eV.

steeply decreases with depth, so the maximum of released deuterium comes from subsurface layers, which explains the position of the first TDS peak near 460 K. The second peak lies near 750 K, which corresponds to the release of deuterium from clusters via bulk diffusion. Activation energy for this process is given by the sum of detrapping and bulk migration energies, and is equal to 2 eV in order to fit the second peak at 750 K (figure 10(*b*)). It does not depend on the depth since the limiting process in this case is detrapping deuterium from clusters rather than facilitating its diffusion to the surface. So,

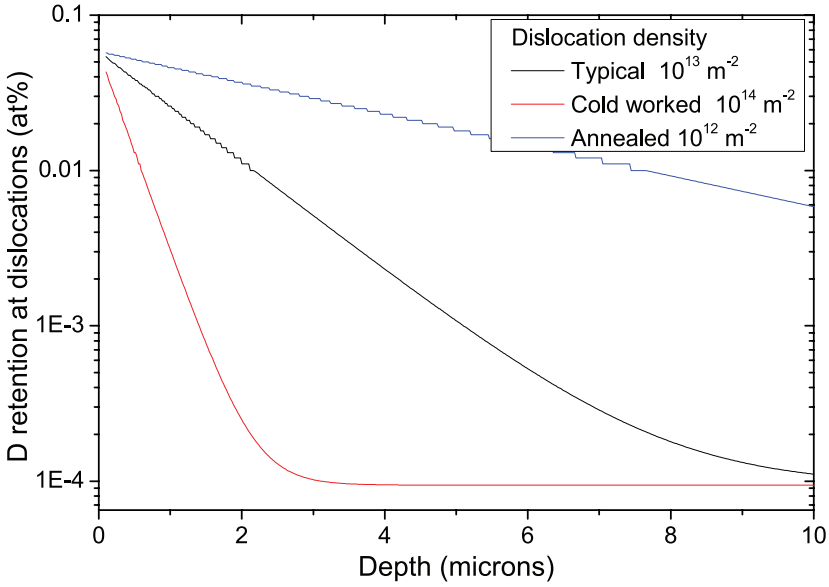

Figure 11. The prediction of the D retention on the dislocation network as a function depth for the same implantation conditions as in figure 6.

taking the D migration energy in bulk E_m^b= 0.4 eV, the detrapping activation energy is estimated as 1.6 eV. This value corresponds well to the H absorption barrier (from vacuum to W bulk) found by DFT to be 1.7 and 2.0 eV for the (100) and (110) surface [5].

Note that the second peak increases with rising implantation time, which implies that large bubbles formed at high fluence cannot be emptied by deuterium release via dislocation channels at the imposed heating rate. Apparently the second mechanism (i.e. emission directly to bulk) comes into play at sufficiently high temperature and competes with the emission via dislocation lines.

5. Conclusions and outlook

We developed a model for D retention in W-based alloys under sub-threshold plasma implantation conditions, assuming the trapping of D at dislocation network. The latter serves not only as the source of trapping, but also as a means for D transport deeper in the bulk. The formulation of the present model was realized with the aid of *ab initio* calculations and experimental estimates deduced from TDS measurements. The model explains the observed saturation of D retention with implantation dose and effects due to alloying of tungsten by tantalum (which essentially changes grain size distribution). Hence, this work provides a link between the kinetics of D retention and microstructural features of the exposed W samples. Further experimental tests may include verification of a strong dependence of the D-penetration depth on the dislocation density. The prediction of the presently developed model for the effect of cold work/deformation on the dislocation-mediated retention is presented in figure 11. The validation of the prediction can be realized by exposure and subsequent nuclear reaction analysis (NRA) measurements, which offers excellent resolution up to a depth of several microns.

As an outlook regarding further development of the microstructure-mediated retention models, we consider that mobility and 'loop-punching' processes on edge dislocations, dislocation junctions and grain boundaries are the primary issues to be assessed. This information will provide a much more accurate description of the nucleation and growth kinetics of D-clusters in a wide range of exposure conditions.

Acknowledgments

V Dubinko acknowledges financial support from Erasmus Mundus (FUSION-EP_0). The work is partially supported by the EUROfusion programme. P Grigorev acknowledges the support from the Erasmus Mundus International Doctoral College in Fusion Science and Engineering (FUSION-DC).

References

[1] Clark R and Reiter D 2005 *Nucl. Fusion Research* (Berlin: Springer)
[2] Frauenfelder R 1968 *J. Vac. Sci. Technol.* **6** 388 Condon J B and Schober T 1993 Nucl. Fusion 207 1
[3] Ahlgren T, Heinola K, Vörtler K and Keinonen J 2012 *J. Nucl. Mater.* **427** 152
[4] Heinola K, Ahlgren T, Nordlund K and Keinonen J 2010 *Phys. Rev.* B **82**
[5] Johnson D F and Carter E A 2010 *J. Mater. Res.* **25** 315
[6] Henriksson K O E, Nordlund K, Krasheninnikov A and Keinonen J 2006 *Fusion Sci. Technol.* **50** 163113
[7] Zayachuk Y, 't Hoen M H J, Zeijlmans van Emmichoven P A, Uytdenhouwen I, and van Oost G 2012 *Nucl. Fusion* **52** 103021
[8] Zayachuk Y, 't Hoen M H J, Zeijlmans van Emmichoven P A, Terentyev D, Uytdenhouwen I and van Oost G 2013 *Nucl. Fusion* **53** 1
[9] Schmid K, Rieger V and Manhard A 2012 *J. Nucl. Mater.* **426** 247
[10] Zhou H B, Liu Y L, Jin S, Zhang Y, Luo G N and Lu G H 2010 *Nucl. Fusion* **50** 025016

[11] Ogorodnikova O V, Roth J and Mayer M 2008 *J. Nucl. Mater.* **373** 254
[12] Haasz A A, Poon M, Macaulay-Newcombe R G and Davis J W 2001 *J. Nucl. Mater.* **290–293** 85
[13] Stephens J 1970 *Metall. Trans.* **1** 1292
[14] Terentyev D, Dubinko V, Bakaev A, Zayachuk Y, Van Renterghem W and Grigorev P 2014 *Nucl. Fus. Lett.* **54** 042004
[15] Kresse G and Hafner J 1993 *Phys. Rev.* B **47** 558
[16] Blochl P E 1994 *Phys. Rev.* B **50** 17593
[17] Perdew J, Wang Y and Engel E 1991 *Phys. Rev. Lett.* **66** 508
[18] Ryazanov A I, Arutyunova G A, Borodin V A, Sikursky Yu N and Chuev V I 1982 *J. Nucl. Mater.* **110** 62
[19] Greenwood G W, Foreman A J E and Rimmer D E 1959 *J. Nucl. Mat.* **4** 505
[20] Dubinko V I, Hu S, Li Y, Henager C H Jr and Kurtz R J 2012 *Phil. Mag.* **92** 4113